EACWE 5
Florence, Italy
19th – 23rd July 2009

Interpretation of aerodynamic pressure measurements by Independent Component Analysis

L.Carassale, A.Vernazzani
Dept. of Civil Environmental and Architectural Engineering, University of Genova
e-mail – luigi.carassale@unige.it
Dept. of Civil Environmental and Architectural Engineering, University of Genova
e-mail – vernazzani@hotmail.it

Keywords: bluff body aerodynamics, pressure fields, proper orthogonal decomposition, independent component analysis, reduced models.

ABSTRACT

A common activity in experimental bluff body aerodynamics is the measurement of pressure fields acting on models by multi-channel scanners. These measurements are often analyzed by multi-variate statistical techniques such as Principal Component Analysis (PCA), more commonly referred as Proper Orthogonal Decomposition (POD), which represents the measurements as a linear combination of deterministic vectors, the PCA modes, modulated by uncorrelated amplitudes. The PCA modes have often been interpreted as elementary pressure patterns, whose characteristics reflect the aerodynamic behavior of the model, and used for interpretation purpose. However, a strong limitation involved in the use of PCA as a pattern identification tool is related to the orthogonality of its modes that, from a physical point of view, is not justifiable. With the purpose of obtaining a representation formula analogous to PCA, but based on a non-orthogonal set of modes, the concept of Independent Component Analysis (ICA) is briefly described and applied to the analysis of pressure measurements carried out of a high-rise building model.

Contact person: L.Carassale, DICAT – University of Genova, Via Montallegro 1 – 16145 Genova, Italy, ph: +39 010 353 2226, FAX: +39 010 353 2534, E-mail: luigi.carassale@unige.it

1. INTRODUCTION

A common activity in experimental bluff body aerodynamics is the measurement of pressure fields acting on models by multi-channel scanners. These measurements are usually idealized as realizations of multi-variate random processes and analyzed by means of statistical approaches usually involving some a-priori assumptions such as stationarity and ergodicity. In this context, one of the most popular techniques is the Principal Component Analysis (PCA), more commonly referred, in bluff body aerodynamics, as Proper Orthogonal Decomposition (POD) (e.g. Solari et al. 2007). According to this technique, a zero-mean N-variate random process is represented by the linear combination of deterministic vectors, referred to as PCA modes, modulated by random processes called Principal Components (PC). PCA possesses three essential properties: 1 – the modes are the eigenvectors of the zero-time-lag covariance matrix of the process and are orthogonal with respect to the Euclidean inner product; 2 – the PC are uncorrelated with each other; 3 – a modal representation based on the PCA modes has the fastest possible convergence in the mean square sense among all the possible linear combinations and therefore can be used to identify reduced-order representations of multi-variate processes.

In practical applications PCA is usually interpreted as a tool for the representation of some specific dataset obtained from an experiment. In this case, the modes are calculated from the sample covariance matrix of the measurements and the PCs are obtained projecting the data on the modes. The number of modes to be retained in the representation is variable from case to case and can be selected on the basis of some convergence criteria; however, the application of PCA to several case-studies demonstrated that the number of modes to be considered is usually very small and that the representation of the pressure field can be obtained by the superimposition of very few modes, which are interpreted as pressure patterns acting on the body with a complete lack of correlation.

From a different point of view, the dominant (with higher variance) modes have often been conceived as convenient tools for the qualitative analysis of pressure fields. The modes are indeed interpreted as elementary pressure patterns, whose characteristics reflect the aerodynamic behavior of the model. Following this approach, it seems natural to ask whether or not the PCA modes have any physical meaning or can separate different physical mechanisms concurring in the generation of the pressure field. These conjectures are encouraged by some interpretations of PCA for which the first mode represents the most recurrent (or typical) deterministic shape hidden in a random phenomenon (Lumley 1970) and by its successful application in several contexts to identify deterministic structures such as dominant eddies (Holmes et al. 1996). In the wind engineering community, it is believed that, even if the PCA modes have some ability in separating some loading contributions (e.g. along-wind and cross-wind forces on symmetrical bodies (Carassale 2009)), their shape do not necessarily resemble any physically consistent pressure distribution (Baker 2000).

A strong limitation involved in the use of PCA as a pattern identification tool is related to the orthogonality of its modes that, from a physical point of view, is not justifiable. The elimination of such a condition, however, is not trivial since it is implicitly embedded in PCA formulation (the modes are the eigenvectors of a symmetric matrix) and, even if it were conceptually possible, it would makes the estimation of the modes undetermined.

With the purpose of obtaining a representation formula analogous to PCA, but based on a non-orthogonal set of modes, the concept of Independent Component Analysis (ICA) is briefly described. This technique has a relatively recent formulation and has been largely employed in several contexts for the solution of the so-called Blind Source Separation (BBS) problem (Hyvärinen et al. 2001). In the wind engineering field, a somehow similar technique called projection pursuit has been applied by Gilliam et al. (2004) for the study of the vortexes emitted by a corner on the roof of a low-rise building; at the authors' knowledge, no other application has been presented.

In bluff-body aerodynamics, ICA can be employed, exactly like PCA, to represent pressure fields acting on a body as a linear combination of deterministic pressure patterns. The application of this technique to the analysis and interpretation of pressure measurements carried out on a prismatic high-rise building model demonstrates its potentialities.

2. MODAL REPRESENTATION OF PRESSURE FIELDS

Let $\mathbf{q}(t)$ be an N-variate stationary random process, function of the time t, representing the pressure field acting on a body, discretised in space according to the experimental setup or the computational mesh. The analysis of the pressure field can be carried out by estimating from the measured data statistical quantities such as correlation functions and probability distribution functions. Besides, the interpretation process often involves the realization of reduced-order representations aimed at reducing the dimension of the data space, emphasizing some desiderated features of the phenomenon. This operation is typically performed by introducing modal representation formulae of the type:

$$\mathbf{q}(t) = \boldsymbol{\mu}_{\mathbf{q}} + \sum_k \boldsymbol{\psi}_k p_k(t) \tag{1}$$

where $\boldsymbol{\mu}_{\mathbf{q}}$ is the expected value of $\mathbf{q}$, $\boldsymbol{\psi}_k$ (k=1,2,…) are deterministic vectors of order N referred to as modes and $p_k(t)$ are stationary random processes. Among the infinite possible modal representations in the form of Eq. (1), the Principal Component Analysis (PCA), often referred to as Proper Orthogonal Decomposition (POD, e.g. Holmes et al. 1996) is by far the most popular choice because of some properties that are briefly recalled in the section below. In the following, without loss of generality, $\mathbf{q}(t)$ will be considered as zero-mean since a possible mean value can be included in the modal representation as in Eq. (1).

2.1 Principal Component Analysis (PCA)

According to PCA, the pressure field $\mathbf{q}(t)$ acting on a body is represented by the modal expansion:

$$\mathbf{q}(t) = \sum_{k=1}^{N} \boldsymbol{\phi}_k x_k(t) = \boldsymbol{\Phi}\mathbf{x} \tag{2}$$

where the vectors $\boldsymbol{\phi}_k$ (k = 1,…,N) are the eigenvectors of the zero-time-lag covariance matrix of $\mathbf{q}$ and are referred to as PCA modes, while x_k are the Principal Components (PC); the matrix $\boldsymbol{\Phi}$ having components $\Phi_{j,k}$ (j, k = 1,…,N) is obtained assembling columnwise the eigenvectors, $\mathbf{x}=[x_1,\ldots,x_N]^{\mathrm{T}}$ and the eigenvectors are enumerated in such a way that their corresponding eigenvalues λ_k are sorted in decreasing order. PCA has the following properties (e.g. Carassale et al. 2007):

1 PCA modes are orthonormal (i.e. $\boldsymbol{\phi}_j^{\mathrm{T}}\boldsymbol{\phi}_k = \delta_{jk}$), thus $\boldsymbol{\Phi}$ is an orthogonal matrix (i.e. $\boldsymbol{\Phi}^{-1} = \boldsymbol{\Phi}^{\mathrm{T}}$) and may be identified as a rotation in $\mathbb{R}^N$;
2 the PC are zero-mean and are uncorrelated with each other (i.e. $\mathrm{E}[x_j(t)\, x_k(t)] = 0$ for $j \neq k$);
3 the variance of the PC is determined by the eigenvalues (i.e. $\mathrm{E}[x_k(t)^2] = \lambda_k$);
4 the first PCA mode $\boldsymbol{\phi}_1$ represents the direction in $\mathbb{R}^N$ as parallel as possible (in the mean square sense) with the vector $\mathbf{q}$, i.e. it maximizes the measure

$$J_1 = \mathrm{E}\left[\left(\boldsymbol{\phi}_1^{\mathrm{T}}\mathbf{q}\right)^2\right] \tag{3}$$

with the constrain $\|\boldsymbol{\phi}_1\|=1$; because of this property, $\boldsymbol{\phi}_1$ is often interpreted as the typical or the most recurrent direction of $\mathbf{q}$;

5 the modal representation given by Eq. (2) has the maximum possible velocity of convergence in the mean square sense; letting

$$\mathbf{q}^{(j)} = \sum_{k=1}^{j} \boldsymbol{\phi}_k x_k \tag{4}$$

then, $\mathbf{q}^{(j)}$ represents the best (in the mean square sense) j-variate approximation of $\mathbf{q}$, i.e. the error measure

$$J_2 = \mathrm{E}\left[\left\| \mathbf{q} - \mathbf{q}^{(j)} \right\|^2 \right] \tag{5}$$

is minimum among all the possible modal representations, while the energy measure

$$J_3 = \mathrm{E}\left[\left\| \mathbf{q}^{(j)} \right\|^2 \right] = \sum_{k=1}^{j} \lambda_k \tag{6}$$

is maximum.

Thanks to the above properties, the reduced-order models derived by PCA are optimal in the mean square sense and may be employed to synthesize the relevant content of experimental datasets fading the noise out.

On the other hand, the perfect lack of correlation between the PCs may suggests that, is **q** is originated by a sum of independent physical causes, then these should remain associated to different modes. Unfortunately, this conjecture is not true since Eq. (2) is only one of the infinite possible linear transformations mapping the vector **q** into a vector with uncorrelated components. The problem of separating different physical causes is addressed in the Section below by means of the Independent Component Analysis (ICA).

2.2 Independent component analysis (ICA)

ICA can be formalized as follows. Let us assume that the random fluctuation of the pressure field **q** is provided by a generative model of the kind

$$\mathbf{q}(t) = \mathbf{A}\mathbf{s}(t) \tag{7}$$

where **s** is a vector of n statistically independent sources s_k ($k = 1,\ldots,n$) said independent components (IC) and **A** is an $N \times n$ full-rank matrix referred to as mixing matrix. The objective of ICA is the estimation of the sources **s** and of the mixing matrix **A**, given the experimental measurements **q**. It is clear that the ICA model (Eq. (7)) is analogous to the representation formula offered by PCA (Eq. (2)), with the difference that the columns $\mathbf{a}_k$ of the matrix **A** are, in general, non-orthogonal and that the ICs s_k are now statistically independent instead of simply uncorrelated like the PCs x_k.

The problem of estimating **s** and **A** form **q** is undetermined since, as it is clear from the structure of Eq. (7), any permutation and scaling of the ICs can be compensated by a suitable permutation and scaling of the columns of **A**. In order to remove such an indetermination, it is assumed that the ICs have unit variance and that are enumerated by sorting the norms of the corresponding columns of **A** in decreasing order.

The estimation of **s** and **A** can be carried out according to different principles including maximum likelihood, mutual information minimization and non-Gaussianity maximization (Hyvärinen et al. 2001). In the following, the latter principle will be applied and justified on a heuristic basis.

According to Eq. (7), the vector **q** is provided by a linear combination of the statistically independent sources s_k; on the other hand, since **q** is in the range of **A**, then an estimator $\tilde{\mathbf{s}}$ for the ICs **s** should be provided by a linear combination of the measurements in the form

$$\tilde{\mathbf{s}}(t) = \mathbf{B}\mathbf{q}(t) \tag{8}$$

Obviously, **B** cannot be directly computed since **A** is unknown; however, relying on Eq. (8) an estimator of an IC s_k can be written in the form

$$\tilde{s}_k = \mathbf{b}^{\mathrm{T}}\mathbf{q} = \mathbf{b}^{\mathrm{T}}\mathbf{A}\mathbf{s} = \mathbf{y}^{\mathrm{T}}\mathbf{s} \tag{9}$$

where $\mathbf{b}^{\mathrm{T}}$ is a row of **B** and the estimator of the IC is expressed as a linear combination of the ICs themselves. Obviously, $\tilde{s}_k$ correctly estimates s_k when **y** is a vector containing all zeros, but a one in the position k.

Eq. (9) cannot be directly used to define the estimator $\tilde{s}_k$ since both **B** and **s** are unknown;

however, it may be argued that, if the ICs have non-Gaussian distribution, due to the central limit theorem, their linear combinations tend to be more Gaussian than the ICs themselves. According to this principle the estimator $\tilde{s}_k$ may be obtained by maximizing the non-Gaussianity of the linear combination $\mathbf{y}^{\mathrm{T}}\mathbf{s}$ with respect the vector $\mathbf{y}$ in $\mathbb{R}^n$. This operation is not possible since $\mathbf{s}$ is unknown, however the same result can be obtained by maximizing the non-Gaussianity of the linear combination $\mathbf{b}^{\mathrm{T}}\mathbf{q}$ with respect to $\mathbf{b}$ in $\mathbb{R}^N$.

The implementation of this principle as an optimization problem requires the definition of a measure for non-Gaussianity; a suitable measure for this purpose is constituted by the neg-entropy (Hyvärinen et al. 2001). The neg-entropy of a scalar-valued random variable y is defined as

$$J[y] = \frac{1}{2} + \log\left(\sqrt{2\pi}\sigma_y\right) + \int p_y(\eta)\log\left(p_y(\eta)\right)\mathrm{d}\eta \tag{10}$$

where p_y and σ_y are, respectively, the probability density function (pdf) and the standard deviation (SD) of y. The integral in Eq. (10), which is extended to the whole definition domain of p_y, represents, if changed of sign, the entropy of the random variable y, while the first two terms provide the entropy of a Gaussian random variable having SD σ_y. Due to the maximum entropy principle (a Gaussian random variable have maximum entropy among all the random variables with the same SD), the neg-entropy is always non-negative and is zero only when y is a Gaussian random variable. Besides, the neg-entropy is invariant with respect the mean and the SD of y.

According to the principle described above, the ICs can be estimated by maximizing the neg-entropy of linear combinations of the type $\mathbf{b}^{\mathrm{T}}\mathbf{q}$, with respect to the vector $\mathbf{b}$ in $\mathbb{R}^N$. From the vectors $\mathbf{b}_j$ corresponding with the relative maxima of the neg-entropy, the matrices $\mathbf{B}$ and $\mathbf{A}$, as well as the ICs $\mathbf{s}$ can be estimated.

In many practical applications, the experimental data do not have any specific physical reason to follow the ICA model given by Eq. (7) (e.g. the pressure field on a body is not necessarily the linear combination of statistically independent sources). However, the application of the estimation procedure described above is still significant since provides a mixing matrix that makes the components of the vector $\mathbf{s}$ as much statistically independent as possible. In this sense, ICA may be interpreted as a modification of PCA in which the orthogonality condition on the modes is substituted by the maximum-independence condition on the coefficients of the linear combination.

A further issue in applying ICA in a practical context is related to the fact that the ICs are equalized (unit variance). As a consequence, all the ICs tend to have similar importance in the description of the pressure field, in contrast with the PCA, which provides the maximum possible velocity of convergence of the modal representation. This implies that ICA is, in general, less efficient than PCA in identifying reduced-order models. In order to circumvent this problem, PCA and ICA is jointly applied: PCA is applied first to reduce the dimension of the data space, projecting the data $\mathbf{q}$ into the space spanned by the first n PCA modes. Then, ICA is applied to the reduced-order version of the data $\mathbf{q}^{(n)}$ (Eq. (4)) or, equivalently, on the vector containing the first n PCs.

Once the ICs and the mixing matrix $\mathbf{A}$ have been estimated, the modal representation provided by ICA can be employed to represent pressure fields acting on a body as a linear combination of deterministic pressure patterns determined by the columns of the mixing matrix $\mathbf{a}_k$, modulated by statistically independent (as much as possible) amplitudes corresponding to the ICs.

3. EXPERIMENTAL APPLICATION

This paragraph compares the results provided by PCA and ICA applied to the pressure field measured on a high-rise building model. The model is prismatic, has square base and aspect ration 1 to 5 (Fig. 1a); the wind flow is characteristic of urban terrain and the Reynolds number is 1.4×10^5 (full details on the experimentation and on the PCA analysis of the whole pressure field acting on the model can be found in Kikuchi et al. (1997)). In the present analysis, only the data measured by the 20 pressure taps at the level of the stagnation point (Fig. 1b) are considered.

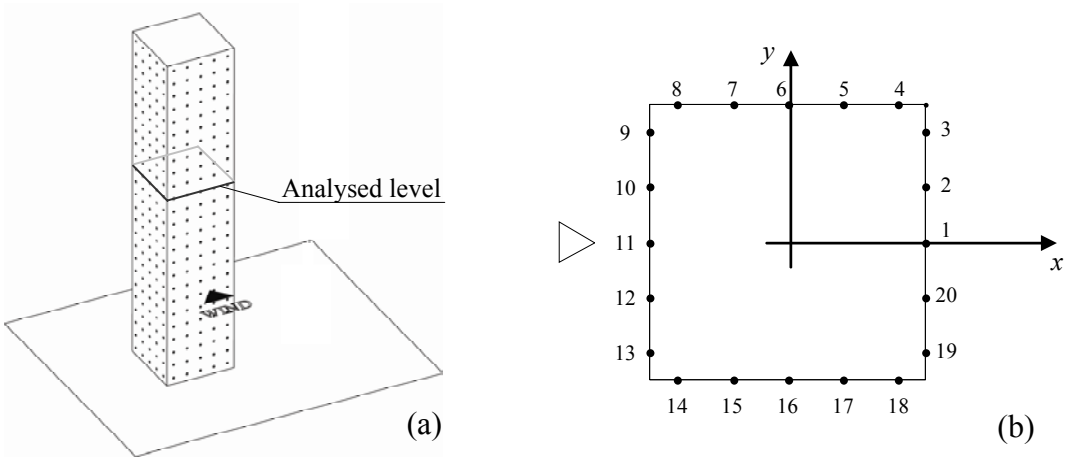

Figure 1: experimental model (a), layout of the pressure taps employed in the analysis (b).

Figure 2 shows the PCA modes estimated from the data. Modes 1 and 3 (Fig. 2a and 2c) are antisymmetric and represent cross-wind and torsional actions, while modes 2, 4, 5 and 6 (Fig. 2b, 2d, 2e and 2d) are symmetric and, as such, produce purely along-wind net forces.

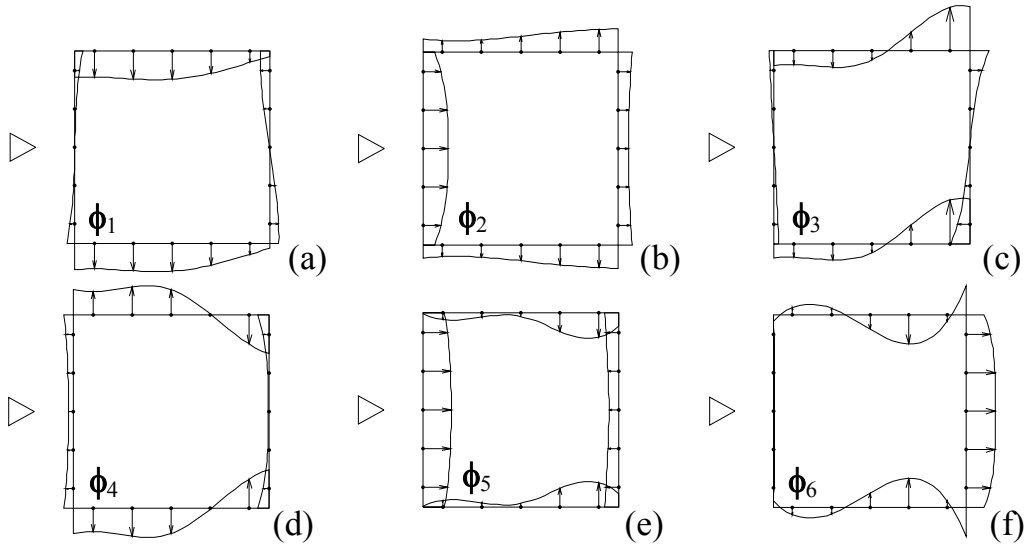

Figure 2: first six PCA modes of pressure field.

Figure 3 shows the convergence, in terms of SD, of the modal representation of the pressure field offered by PCA. Figures 3a to 3c show, respectively, the convergence of the norm of the pressure field ($\|\mathbf{q}\|$, Fig. 3a) and of the local pressure field in two positions on a lateral face of the model, immediately after the windward corner (q_{14}, Fig. 3b) and immediately before the leeward corner (q_{18}, Fig. 3c). Figures 3d to 3f show, respectively, the convergence of the generalized forces $f_x^{(j)}$, $f_y^{(j)}$ and $m_z^{(j)}$ produced by the pressure field $\mathbf{q}^{(j)}$. The pressure field $\mathbf{q}^{(6)}$ represented through the six modes reported in Figure 2 approximates the actual pressure field representing 93% of the SD of its norm, 95% and 96% of the SD of the pressure measured by pressure taps 14 and 18, respectively, 99% of the along-wind force SD, 100% of the cross-wind force SD and 87% of the torsional moment SD. As it was already noted by Kikuchi et al. (1997), the torsional moment has slower convergence with respect to the other generalized forces; besides, it is worth noting that 99% of the cross-wind force SD is provided by the first mode (Fig. 2a).

In spite of the excellent convergence observed in Figure 3 and of the successful separation of

along-wind and cross-wind/torsional contributions, which is due to the symmetry of the test condition (Carassale 2009), the use of these modes as interpretative tools for describing the pressure field is troublesome. Indeed, some features of the modes seem not to be consistent with the known physical phenomenon. In particular, mode 1 (Fig. 2a) presents pressure distributions deterministically equal (with opposite sign) on the two lateral faces of the model, while, it is well known that the suction generated by vortex shedding tends to be quite more intense than the compression appearing on the opposite face. Besides, mode 4 (Fig. 2d) represents a pressure distribution acting on the lateral faces that is somehow compatible with the formation of recirculation bubbles after the windward corners and the re-attachment of the boundary layer on the lateral faces just before the leeward corners; unfortunately, mode 4 represents the synchronous realization of this mechanism on both the lateral faces of the model, while, at the Reynolds number reproduced in the experimentation, the vortex shedding is expected to be alternate. An effort to identify a physical interpretation of modes 3, 5 and 6 does not seem reasonable.

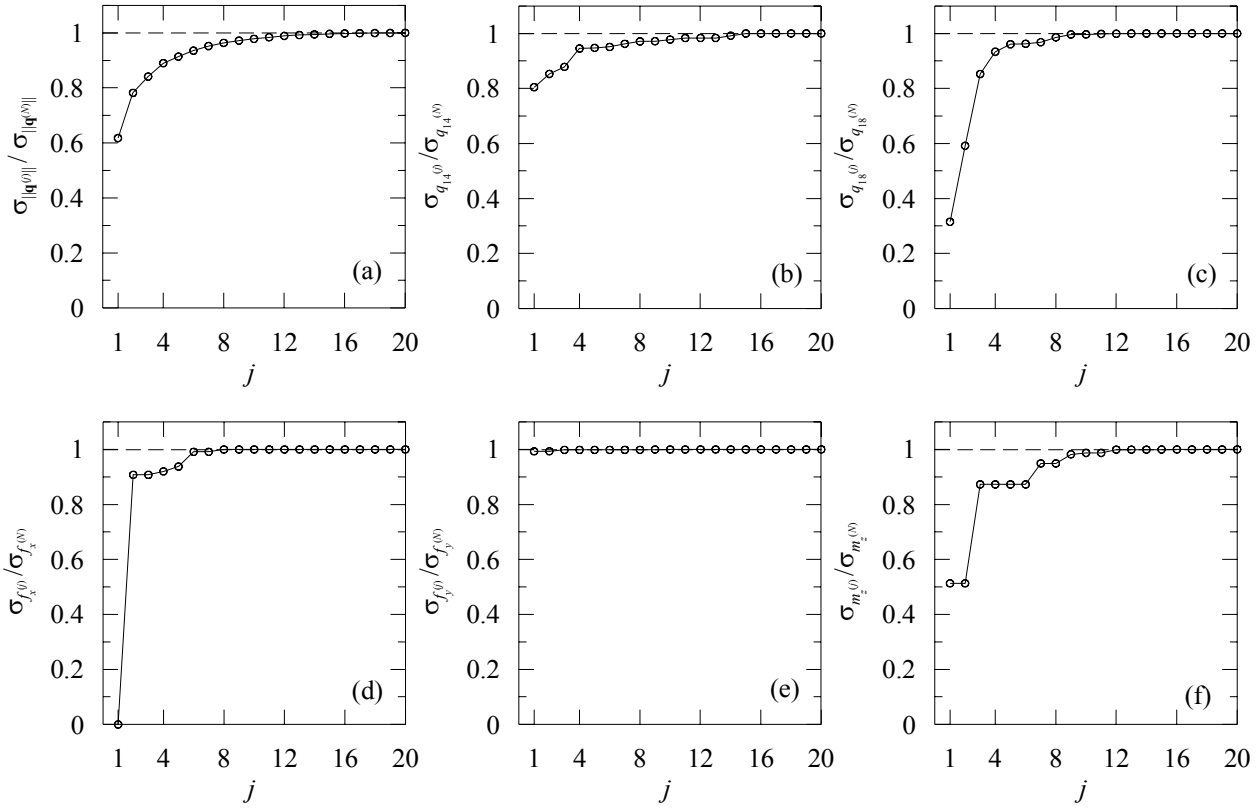

Figure 3: convergence of the representation of the pressure field in terms of norm (a), SD of the local values at location 14 (b) and 18 (c), along-wind force (d), cross-wind force (e), torsional moment (f).

Figure 4 shows the ICA modes obtained by the reduced-order pressure field $\mathbf{q}^{(6)}$ defined by the first six PCA modes. In this representation, the cross-wind action is determined by four modes, two for a lateral face and two for the other one. Mode 1 (Fig. 4a) represents an intense suction after the windward corner on the left lateral face and a weak compression on the opposite face; mode 2 (Fig. 4d) represents the pressure field symmetrical to mode 1. Modes 3 and 4 represents pressure distribution acting on the lateral faces (left and right, respectively) having their maximum value near the leeward corner. ICA modes 5 and 6 practically coincide with PCA modes 2 and 6 and mainly represent pressure distributions on the windward and leeward face, respectively. While in PCA representation the cross-wind action is completely contained in the first mode, in ICA representation the modes 1 to 4 contribute to the cross-wind force roughly with the same importance (the IC are unit

variance, hence the importance of the modes is entirely due to their modal amplitude). This higher dimension of the space employed to represent the cross-wind action reflects in a better ability of ICA in identifying relevant physical mechanisms. In particular, unlike in the case of PCA, ICA modes do not imply a deterministic relationship between the pressure acting on the two lateral faces, enabling a more correct mono-variate representation of the pressure field on the lateral faces due to vortex shedding.

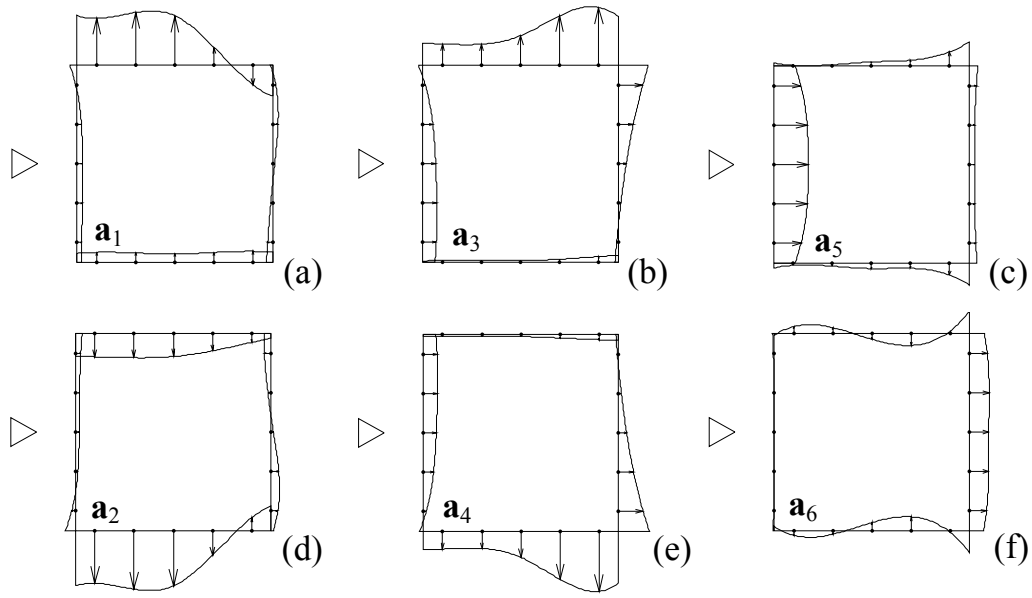

Figure 4: ICA modes spanning the space defined by the first six PCA modes (Fig. 2).

Figure 5 shows the SD of the measured pressure field (solid line) and its representation by the first PCA mode $\boldsymbol{\phi}_1$ (Fig. 5a, dashed line) and through the ICA mode $\mathbf{a}_2$ (Fig. 5b, dashed line); in the location of the pressure tap 14, they provide, respectively, 80% and 88% of the actual SD.

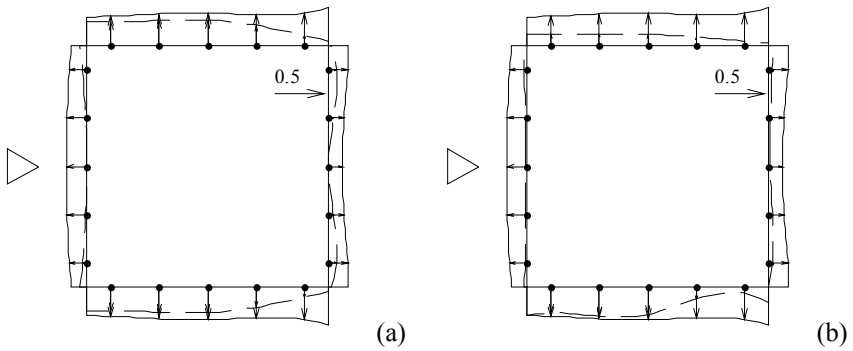

Figure 5: Standard deviation of the mono-variate representation of the pressure field obtained by PCA mode 1 (a) and ICA mode 2 (b).

Figure 6 shows the PSD (a) and the pdf (b) of the pressure coefficient q_{14}, measured by a pressure tap located just after a leeward corner (Fig. 1b) (solid lines), of the PC x_1 (dashed line) and of the IC s_2 (dash-dot line) whose respective modes provide most of the contribution to the representation of the pressure field in the neighborhood of tap 14 (Figs. 2 and 4). For the comparison, the pressure coefficient and the PC are standardized, i.e., $\hat{q}_{14} = q_{14} / \sigma_{q_{14}}$, $\hat{x}_1 = x_1 / \lambda_1^{0.5}$. Both the considered PC and the IC have a spectral peak about the reduced frequency $8 \cdot 10^{-2}$, consistently with the pressure coefficient measured just after the leeward corners (the frequency is non-dimensionalized by the size of the model cross section b and the undisturbed wind velocity U). From the comparison it appears

that the PSD of the PC is more focalized at the peak frequency while the IC has higher power in the low frequency range. Form the observation of the pdf (Fig. 6b) it emerges that the probability distribution of the IC s_2 is very similar to the probability distribution of the pressure coefficient q_{14}, but is quite different from the probability distribution of x_1, which, due to symmetry reasons, necessarily has a symmetric pdf (Carassale 2009).

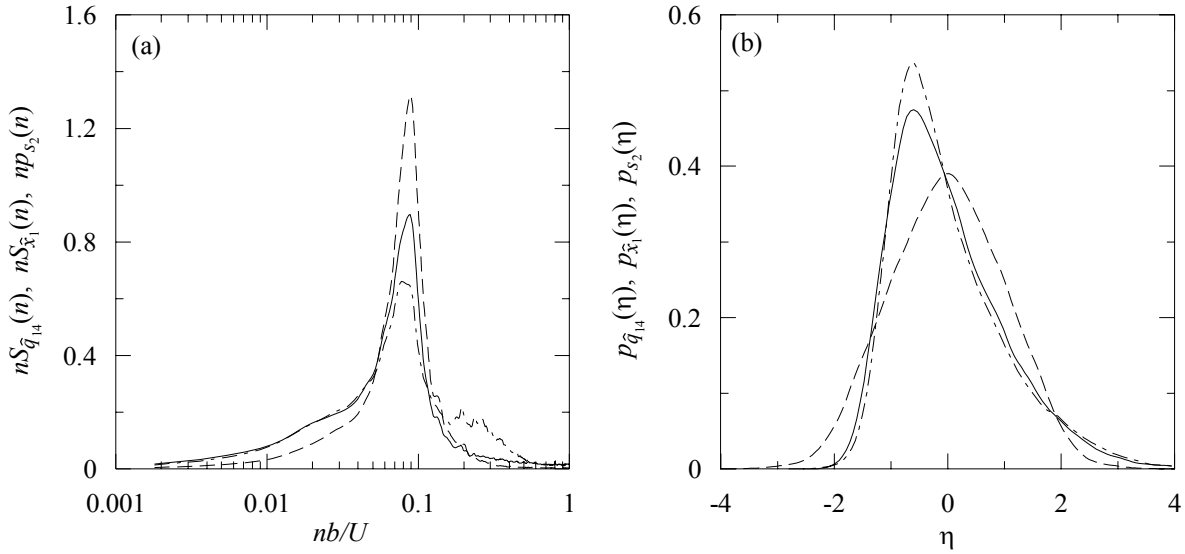

Figure 6: PSD (a) and pdf (b) of the standardized pressure coefficient q_{14} (solid line), standardized PC x_1 (dashed line) and IC s_2 (dash-dot line).

The difference between the probability distribution of x_1 and s_2 emerged in Figure 6b reflects in a different ability of PCA and ICA in realizing a mono-variate approximation of determined regions of the pressure field. To point out this difference, Figure 7 shows a portion of a time history of the pressure coefficient q_{14}, compared to the mono-variate approximation obtained by PCA (Fig. 7a) and ICA (Fig. 7b). As it can be observed, a single ICA mode (mode 2, in this case) approximates accurately the measured time history, while PCA regularly underestimate the positive peaks (suction) and overestimate the negative peaks (compression) due to the symmetry of its probability distribution.

Figure 8 shows the PSD (a), the coherence function (b) and the phase delay (c) of the ICs s_1 and s_2 (Figs. a.1, b.1, c.1) and of the ICs s_1 and s_3 (Figs. a.2, b.2, c.2). The ICs s_1 and s_2 correspond to modes mainly contributing to the representation of the pressure filed on the lateral faces of the model just after the leeward corners (Fig. 4) and have similar PSD with a spectral peak at a reduced frequency about $8 - 9 \cdot 10^{-2}$. Their coherence at the peak frequency is about 0.5 with a phase delay about π. These results indicate that the pressure fields represented by the ICA modes 1 and 2 fluctuate, at the vortex shedding frequency, with negatively-correlated amplitudes. In other words, when a suction (positive IC) appears at a side of the model, at the opposite side a compression is likely to appear. The ICA mode 3 represents a pressure distribution having its higher amplitude on the same lateral face than mode 1 (Fig. 4), but near the leeward corner. Its PSD has a peak at a reduced frequency about 0.1 (i.e. slightly higher than mode 1); in this frequency range the coherence is very high (about 0.8) and the phase delay is about 0.2π. This phase angle roughly coincides with the time necessary to cover a distance about 1.4 times the size of the model at the velocity of the undisturbed flow. This time seems to be compatible with the velocity of a vortex generated at the windward corner and advected along the lateral face of the model.

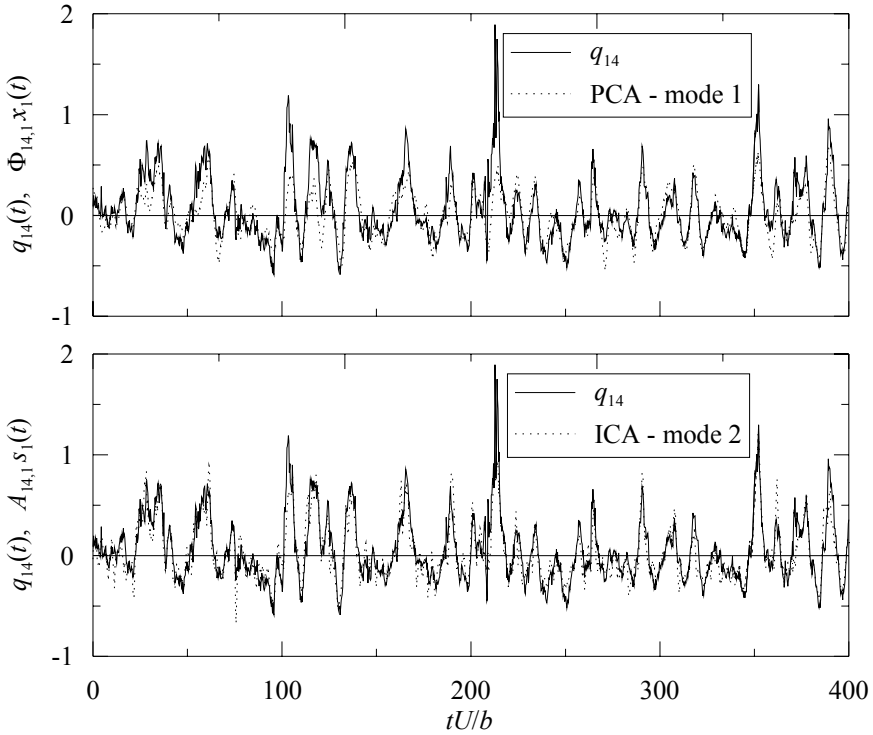

Figure 7: time histories of the pressure coefficient q_{14} (solid line) and its approximation by PCA mode 1 (a) and ICA mode 2 (b).

Figure 9 shows the joint probability density function (jpdf) of the ICs s_1 and s_2 (Fig. 9a) and of the ICs s_1 and s_3 (Fig. 9b). The jpdf of s_1 and s_2 is structured in such a way that large positive values of s_1 tend to appear jointly with small values for s_2 and vice versa. This statistical property, together with the phase delay observed in Figure 8c.1 suggests that the ICs s_1 and s_2 represent intense suctions and weak compressions appearing alternately on the two sides of the model. Figure 9b shows the jpdf of $s_1(t)$ and $s_3(t+\tau)$, with τ being the time lag corresponding to the phase delay observed in Figure 8c.2 at the peak frequency. It can be noted that the s_1 and s_3 are well correlated at the time lag τ, indicating that the pressure field represented by mode 3 may be considered as the evolution of the pressure field represented by mode 1. From a physical point of view, it may be argued that mode 1 represents the generation of the recirculation bubble and the re-attachment of the boundary layer, while mode 3 may be consistent with the pressure field generated by vortex advected towards the leeward corner. Modes 2 and 4 have the same role on the opposite face of the model.

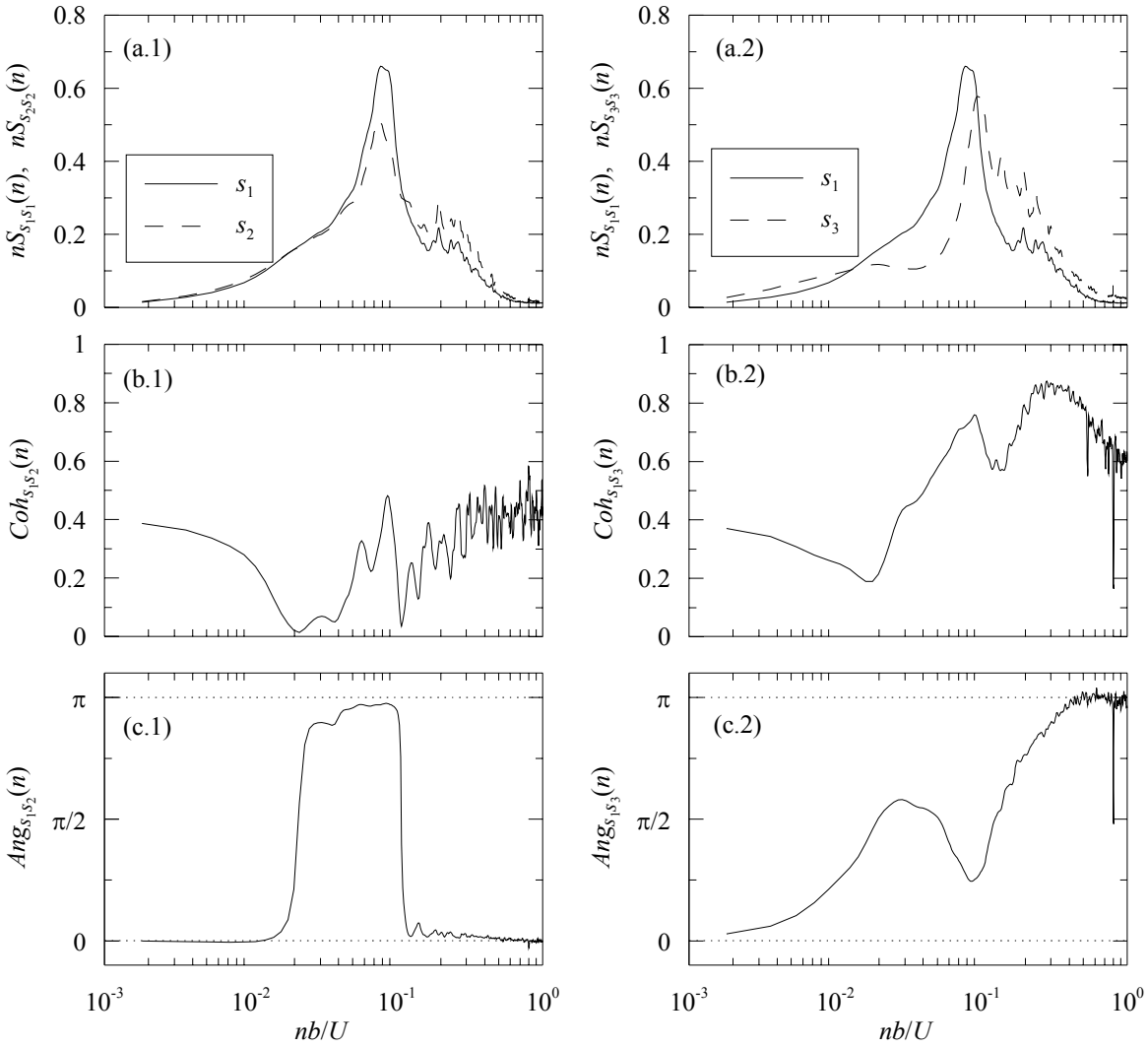

Figure 8: PSD (a), coherence function (b), and phase delay (c) of the ICs s_1 and s_2 (a.1, b.1 c.1) and of the ICs s_1 and s_3 (a.2, b.2, c.2).

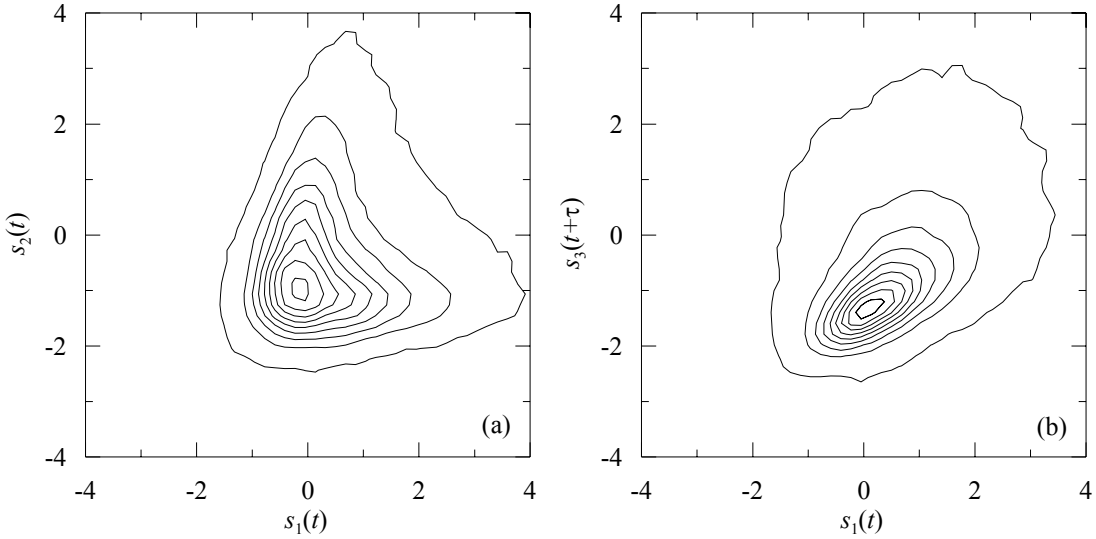

Figure 9: joint probability density function of the ICs s_1 and s_2 at zero time lag and of the ICs s_1 and s_3 at the time lag corresponding to phase delay observed in Fig. 8b.3 at the peak frequency (b).

4. CONCLUSIONS

ICA can be employed to realize modal representations of pressure fields in alternative to the traditional PCA. From the analysis of a practical application it emerges that ICA modes result more consistent with the physical phenomenon under investigation and are more efficient in realizing low-dimensional models of local pressure fields in the regions characterized by the separation of the boundary layer.

Referring to the particular case examined herein, the qualitative differences between ICA and PCA representations can be summarized as follows:

1 ICA modes are consistent with an alternate vortex shedding having the suction phase more intense than the compression phase (modes 1 and 2); PCA representation suggests the realization of an alternate vortex shedding mechanism in which suction and compression have the same intensity (mode 1);
2 the pdf of the ICs s_1 and s_2 corresponding to the pressure fields on the lateral faces near the windward corners are consistent with the pdf of the local pressure fields; on the contrary the pdf of the PC x_1 responsible of most of the pressure fluctuation on the lateral faces is very far from the local pressure pdf;
3 the time series of the local pressure on the lateral faces is better represented by a single ICA mode that by a single PCA mode;
4 the two ICA modes representing the pressure field on each lateral face of the model are related in such a way to represent the advection of vortexes towards the leeward corners; this mechanism is not identifiable from the observation of the PCA modes.

ACKNOWLEDGMENTS

The experimental data discussed in this paper were obtained in the Shimizu Corporation Laboratories, as documented in Kikuchi et al. 1997. The scientific support offered by Prof. Yukio Tamura and the work of all the researchers involved in mentioned project is gratefully acknowledged.

REFERENCES

Baker, C.J. (2000), “Aspects of the use of proper orthogonal decomposition of surface pressure fields”, Wind & Struct., 3, 97-115.

Carassale L., Solari G. e Tubino F. (2007). Proper Orthogonal Decomposition in Wind Engineering: Part 2: Theoretical Aspects and Some Applications, Wind & Struct., 10(2), 177-208.

Carassale, L. (2008). Flow-induced forces on cylinders in statistically-symmetric cross flow, Prob. Engrg. Mech., 24(3), 323-339.

Gilliam X., Dunyak J.P., Smith D.A. Wu, F. (2004). “Using projection pursuit and proper orthogonal decomposition to identify independent flow mechanisms”, J. Wind Engng. Ind. Aerodyn, 92, 53-69.

Hyvärinen A., Karhunen J., Oja E. (2001). *Independent component analysis*. John Wiley and Sons, New York.

Holmes P., Lumley J.L., Berkooz G. (1996). *Turbulence: coherent structures, dynamical systems and symmetry.* Cambridge University Press, Great Britain.

Kikuchi H., Tamura Y., Ueda H., Hibi K. (1997). “Dynamic wind pressure acting on a tall building model - Proper orthogonal decomposition”. Journal of Wind Engineering and Industrial Aerodynamics, 69-71, 631-646.

Lumley, J.L. (1970). *Stochastic tools in turbulence*. Academic Press, New York.

Solari G., Carassale L., Tubino F. (2007). “Proper Orthogonal Decomposition in Wind Engineering: Part 1: A State-of-the-Art and Some Prospects”, Wind and Structures, 10(2), 153-176.